



Published in final edited form as:

Cancer Discov. 2022 May 02; 12(5): 1233–1247. doi:10.1158/2159-8290.CD-21-1119.

Zenocutuzumab, a HER2xHER3 bispecific antibody, is effective therapy for tumors driven by NRG1 gene rearrangements

Alison M. Schram^{1,2,*,#}, Igor Odintsov^{3,4,*}, Madelyn Espinosa-Cotton⁵, Inna Khodos⁶, Whitney J. Sisso³, Marissa S. Mattar⁶, Allan J.W. Lui³, Morana Vojnic^{3,4,\$}, Sara H. Shameem¹, Thrusha Chauhan¹, Jean Torrisi⁷, Jim Ford⁸, Marie N. O'Connor⁸, Cecile A.W. Geuijen⁸, Ron C. J. Schackmann⁸, Jeroen J. Lammerts van Bueren⁸, Ernesto Wasserman⁸, Elisa de Stanchina⁶, Eileen M. O'Reilly^{1,2}, Marc Ladanyi^{3,4}, Alexander Drilon^{1,2}, Romel Somwar^{3,4,#}

¹Department of Medicine, Memorial Sloan Kettering Cancer Center, New York, NY 10065, USA

²Weill Cornell Medical College, New York, NY 10065, USA

³Department of Pathology, Memorial Sloan Kettering Cancer Center, New York, NY 10065, USA

⁴Human Oncology and Pathogenesis Program, Memorial Sloan Kettering Cancer Center, New York, NY 10065, USA

⁵Department of Pediatrics, Memorial Sloan Kettering Cancer Center, New York, NY 10065, USA

⁶Anti-tumor Core Facility, Pharmacology Program, Memorial Sloan Kettering Cancer Center, New York, NY 10065, USA

⁷Department of Radiology, Memorial Sloan Kettering Cancer Center, New York, NY 10065, USA

⁸Merus N.V., Utrecht, the Netherlands

Abstract

NRG1 rearrangements are recurrent oncogenic drivers in solid tumors. *NRG1* binds to *HER3*, leading to heterodimerization with other *HER/ERBB* kinases, increased downstream signaling, and tumorigenesis. Targeting *ERBBs*, therefore, represents a therapeutic strategy for these cancers. We investigated zenocutuzumab (Zeno, MCLA-128), an ADCC-enhanced anti-*HER2xHER3* bispecific antibody, in *NRG1* fusion-positive isogenic and patient-derived cell lines and xenograft models. Zeno inhibited *HER3* and *AKT* phosphorylation, induced expression of apoptosis markers, and inhibited growth. Three chemotherapy-resistant *NRG1* fusion-positive metastatic cancer patients were treated with Zeno. Two patients with *ATP1B1-NRG1*-positive pancreatic cancer achieved rapid symptomatic, biomarker, and radiographic responses, and remained on treatment for over 12 months. A *CD74-NRG1*-positive NSCLC patient who had progressed on six prior lines of systemic therapy including afatinib responded rapidly to treatment with a partial

Authors for Correspondence: Alison M. Schram, MD, Department of Medicine, Memorial Sloan Kettering Cancer Center, 300 East 66th Street, New York, NY 10064. Tel: 646-888-5388. schrama@mskcc.org, Romel Somwar, PhD, Department of Pathology, Memorial Sloan Kettering Cancer Center, 1275 York Ave, New York, NY, 10065. Tel: 212-639-2000. somwarr@mskcc.org.

*These authors contributed equally to this work

\$Current address: Lenox Hill Hospital, Northwell Health, NY, NY, 10075, USA

response. Targeting HER2 and HER3 simultaneously with Zeno is a novel therapeutic paradigm for patients with NRG1 fusion-positive cancers.

Keywords

antibody therapy; heregulin; patient-derived xenografts; tumor-agnostic biomarker; precision medicine

Introduction

Genomic rearrangements involving the neuregulin 1 gene (*NRG1*) have been identified across several solid tumor types, including lung, breast, pancreas, ovarian, and prostate cancer (1–7). *NRG1* fusions are specifically enriched in *KRAS*-wildtype pancreatic cancer (7,8) and *KRAS*-wildtype invasive mucinous adenocarcinoma (IMA) (6,9,10), where they are believed to be mitogenic drivers. Chromosomal abnormalities involving *NRG1* were first identified in 1998 in breast cancer (11), and *NRG1* gene fusions were first described in 1999 in the breast cancer cell line MDA-MB-175-VII (12,13). Chimeric *NRG1* proteins contain an upstream fusion partner and retain the EGF-like domain of *NRG1*, which confers ligand binding and transformation (14,15) via the ERBB family of receptor tyrosine kinases (RTKs).

The ERBB RTK family consists of EGFR (ERBB1), HER2 (ERBB2), HER3 (ERBB3), and HER4 (ERBB4); these RTKs are often exploited by cancer cells to promote growth in solid tumors (16,17). In addition to stimulation by *NRG1* fusion proteins, oncogenic activation of ERBB receptors may occur directly through mutations and translocations that confer constitutive enzymatic activity (e.g. EGFR and HER2 kinase domain mutations, EGFRvIII variant where the extracellular region of the RTK is deleted, and EGFR fusions). Such activation can also arise through gene amplification (e.g. *EGFR* and *HER2*) or protein overexpression. The identification of *NRG1* chimeric ligands has led to increasing attention to constitutive ligand-induced activation and a search for therapeutics that can interfere with *NRG1* action.

NRG1 binds primarily to HER3 and HER4 (18,19), leading to heterodimerization or oligomerization with other ERBB family members. HER3 is a pseudokinase with little, if any, intrinsic enzymatic activity, making it a dependent heterodimerization partner that relies on phosphorylation from other ERBB members (20). *NRG1*-mediated activation of HER3 promotes asymmetric dimerization with EGFR, HER2 and HER4 (20). These partners phosphorylate HER3, forming docking sites for SH2-domain proteins, leading to activation of multiple signal transduction pathways, including the phosphoinositide 3-kinase (PI3K) pathway, culminating in cell proliferation and survival. In an experimental system in which only EGFR and HER3 are expressed, stimulation with *NRG1* leads to phosphorylation of HER3 but not of EGFR; however, when only HER2 and HER3 are expressed, *NRG1* induces phosphorylation of both HER2 and HER3 (21). Although the mechanism of HER2 phosphorylation in this context is unclear, it is thought that *NRG1* triggers higher order oligomerization that leads to collateral HER3-HER3 interactions (21,22). The HER2-HER3 dimers may represent the most oncogenic heterodimers of the ERBB family (23). Targeting

HER2-HER3 signaling therefore represents a promising therapeutic approach for patients with NRG1 fusion-positive malignancies.

Reports of effective HER2 and/or HER3 targeting in xenograft models and in patients with IMA, cholangiocarcinoma, and pancreas cancer harboring *NRG1* rearrangements have fueled interest in exploiting these RTKs as therapy for this molecularly defined cancers (6,7,10,24–27). Clinical responses to the pan-ERBB tyrosine kinase inhibitor, afatinib (10,24), and the anti-HER3 antibody, GSK2849330, have been described in retrospective reports (24). However, no published prospective clinical trials have evaluated the efficacy of these agents in NRG1 fusion-positive cancers.

Zeno (zenocutuzumab, MCLA-128) is a bispecific humanized immunoglobulin G1 (IgG1) containing two different Fab arms, targeting extracellular domains of HER2 and HER3 (26). The HER2-targeting arm binds to the more abundant HER2 protein on the cell surface. In addition to providing a high local concentration of the antibody, this action positions the HER3-targeting arm to block NRG1 binding to HER3 and prevent HER3 from undergoing the conformational change required for heterodimerization with HER2 and potentially with EGFR (26). This unique so-called ‘dock’ (HER2 arm) and ‘block’ (HER3 arm) mechanism prevents the subsequent phosphorylation of the cytoplasmic domain of HER3 and downstream oncogenic signaling (26). Further, glycoengineered modification of the IgG1 to augment affinity for Fc receptors results in enhanced antibody-dependent cellular cytotoxicity (ADCC) (26). The safety and tolerability of Zeno has previously been demonstrated in a phase I study (28). Here we report the therapeutic efficacy of Zeno *in vitro* and *in vivo* in preclinical models of lung, breast, pancreas, and ovarian cancers harboring *NRG1* fusions. Moreover, we demonstrate clinical efficacy in patients with lung and pancreatic cancers driven by *NRG1* rearrangements. These results support the use of Zeno as therapy for NRG1 fusion-driven cancers of any histology in an ongoing phase I/II trial (NCT02912949).

Results

Zeno effectively inhibits growth of lung and breast cancer cell lines with *NRG1* alterations

We examined the effect of the bispecific HER2xHER3 antibody, Zeno, on growth of a panel of patient-derived and isogenic cell lines expressing various *NRG1* fusions. Details of the cell lines are provided in Supplementary Fig. S1. While the patient-derived cell lines allowed us to examine Zeno efficacy in models representing the genomic complexity of tumors, Zeno specificity could be demonstrated in the isogenic cell lines by comparing *NRG1*-rearranged cells with control cells. Growth of isogenic human bronchiolar epithelial cell lines (HBEC) expressing either CD74-NRG1 or VAMP2-NRG1 fusions was reduced by sub-nanomolar concentrations of Zeno (Fig. 1A). In contrast, growth of the isogenic control HBEC line remained largely unaffected by Zeno treatment, with maximum inhibition of approximately 25% at the highest concentration used (Fig. 1A). Comparison of the IC₅₀ values for inhibition of cell growth by Zeno revealed that HBEC cells with NRG1 fusions were approximately 40,000 times more sensitive to Zeno than the parental control cells (see Supplementary Fig. S2A for IC₅₀ values), consistent with oncogene addiction. Similar to the HBEC-NRG1 cell lines, growth inhibition of the lung adenocarcinoma cell line

LUAD-0061AS3 (SLC3A2-NRG1) (29) occurred with low nanomolar concentrations of Zeno (IC_{50} =14.2 nmol/L) (Fig. 1B and Supplementary Fig. S2A).

Given the high sensitivity of *NRG1*-fusion positive lung cancer cell lines to Zeno, we sought to examine the efficacy of this antibody in breast cancer cell lines with *NRG1* fusions. We generated an isogenic pair of cell lines by ectopic expression of *DOC4 (TENM4)-NRG1* cDNA in the breast cancer cell line MCF7. Expression of *NRG1* fusions were confirmed by western blotting (Supplementary Fig. S2B, left panel). Zeno treatment inhibited growth of MCF7-DOC4-NRG1 cells with an IC_{50} value of 2.01 nmol/L but had little effect on growth of the isogenic control line MCF7-EV (IC_{50} =4811 nmol/L) (Supplementary Fig. S2C). We also examined a breast cancer cell line with an *NRG1* fusion, MDA-MB-175-VII, which expresses a complex *NRG1* fusion involving three genes (*PPP6R3-TENM4-NRG1*) (30). Of all the cell lines tested, MDA-MB-175-VII was the most sensitive to Zeno treatment with an IC_{50} value of 0.04 nmol/L (Fig. 1C and Supplementary Fig. S2A). Finally, we examined the effect of Zeno treatment on growth of the lung cancer cell line HCC-95, which harbors *NRG1* amplification (24). Similar to the *NRG1* fusion positive lung and breast cancer cell lines, growth of the HCC-95 cell line was also reduced by Zeno (IC_{50} = 0.15 nmol/L) (Supplementary Fig. S2A and S2D). These results indicate that Zeno effectively blocks growth of cells with *NRG1* alterations at low or sub-nanomolar concentrations, with comparably little effect on the growth of isogenic control cells lacking *NRG1* alterations.

Zeno blocks transmission of downstream proliferation signals in lung and breast cancer cell lines

To further characterize the cellular mechanisms by which Zeno blocks growth of *NRG1*-rearranged cell lines, we looked at the transmission of intracellular signals believed to regulate proliferation and survival in cells treated with the antibody. We found that exposure of HBEC-CD74-NRG1, LUAD-0061AS3, and MDA-MB-175-VII cells to Zeno resulted in a dose-dependent reduction in the phosphorylation of HER3, HER2, and HER4 (Fig. 1D-F). Similarly, Zeno treatment also inhibited phosphorylation of other downstream effectors of these receptor tyrosine kinase pathways including STAT3, AKT, p70S6K, and S6. In HBEC-CD74-NRG1 cells, 1 nmol/L Zeno led to substantial reduction in HER3 and AKT phosphorylation (Fig. 1D). EGFR phosphorylation was also reduced, mainly in LUAD-0061AS3 and MDA-MB-175-VII cells (Fig. 1E and 1F). Zeno treatment reduced MEK and ERK phosphorylation in LUAD-0061AS3 cells, but less so in the other two cell lines (Fig. 1D-F). Similar results were obtained in the HCC-95 cell line in which *NRG1* is amplified (Supplementary Fig. S3A). In the fusion-negative control cells, treatment with Zeno reduced phosphorylation of HER3 and HER2 at 0.1 and 10 nmol/L concentrations, respectively (Supplementary Fig. S3B-C). However, this did not translate to effective inhibition of downstream signaling (Supplementary Fig. S3B-C), as seen with the isogenic counterpart harboring CD74-NRG1 or other cell lines harboring *NRG1* fusions (Fig. 1D-F). Protein expression was not altered by the 1.5 h Zeno treatment in any of the cell lines. Taken together, these results demonstrate that 0.1–100 nM Zeno potently inhibits the HER3-AKT-mTOR pathway in cell lines harboring *NRG1* fusions or amplification.

Zeno treatment induces markers of apoptosis and cell cycle arrest in lung and breast cancer cell lines

To delineate the mechanism by which Zeno treatment may inhibit growth, we treated cells with *NRG1* alterations for up to 48 hours with 50 nmol/L Zeno and determined expression of phosphorylated HER3, AKT, ERK, and S6 ribosomal protein over time, as well as that of markers of cell cycle progression and apoptosis. In the two cell lines with *NRG1* fusions and the *NRG1*-amplified HCC-95 cell line, phosphorylation of HER3, AKT, and S6 was almost completely shut down by 3 h, and remained suppressed throughout the 48 h time period of the experiment (Supplementary Fig. S4A; Some of these blots were presented previously at the AACR 2021 scientific meeting). However, phosphorylation of ERK started to rebound by 16 h of treatment in the LUAD-0061AS3 cell line. In MDA-MB-175-VII cells, ERK phosphorylation was already as high as basal level at the 3 h after treatment (the shortest time point in these time-course studies). Prolonged treatment with Zeno did not affect the levels of total HER3, AKT, or ERK (Supplementary Fig. S4A). Increased expression of apoptosis markers (Supplementary Fig. S4A) was also observed. Enhanced levels of cleaved PARP (c-PARP) were evident as early as 3 h after treatment began, and continued to increase for the entire period of the experiment. Increased BIM expression was observed in all cell lines, with the BIM_{EL} isoform being the most responsive in the two cell lines harboring inactivating p53 mutations (LUAD-0061AS3 and HCC-95). Upregulation of PUMA in response to Zeno treatment was observed mainly in MDA-MB-175-VII cells (wildtype p53) within 3 h of incubation, reaching a maximum by 16 h; this high level was sustained for the rest of the 48 h treatment time. Exposure to Zeno led to an increase in the p27 (CDKN1B) cell cycle inhibitor and a decrease in the cyclin D1 (CCND1) protein that permits progression through the G1 phase of the cell cycle. Levels of the p21 cell cycle inhibitor (CDKN1A) remained unchanged in the LUAD-0061AS3 and MDA-MB-175-VII cell lines until the final time point (48 h) when a decrease was observed (Supplementary Fig. S4A). However, in HCC-95 cells, p21 levels increased in response to Zeno treatment (Supplementary Fig. S4A). Treatment of MDA-MB-175-VII and LUAD-0061AS3 cells with Zeno resulted in a dose-dependent increase in caspase 3/7 enzymatic activity (Supplementary Fig. S4B), supporting the results from western blotting that Zeno treatment induces apoptosis. These results indicate that Zeno is capable of sustained HER3 inhibition, blockade of the cell cycle, and induction of apoptosis.

Zeno treatment induces antibody-dependent cellular cytotoxicity (ADCC)

Zeno is an IgG1 subtype antibody designed to induce enhanced antibody-dependent cellular cytotoxicity (ADCC) through afucosylation of the Fc (26). Here, we examined Zeno for ADCC activity using peripheral blood mononuclear cells in a chromium release assay. MDA-MB-175-VII and HCC-95 cells were loaded with ⁵¹Cr and then incubated with peripheral blood mononuclear cells. The amount of ⁵¹Cr released by the tumor cells indicates cytotoxicity. We observed a significant increase in cytotoxicity of the MDA-MB-175-VII and HCC-95 cells in the presence of Zeno, but not in the presence of non-specific IgG1 molecules (Supplementary Fig. S5A-B). Moreover, Zeno induced a level of cytotoxicity that was higher than that caused by the anti-HER2 antibody trastuzumab. These results confirm that Zeno can induce ADCC in cells with *NRG1* fusions or amplification. Similar results have been shown previously for Zeno in SKBR-3 cells (26).

Zeno is effective at blocking NRG1 fusion-dependent signaling and growth in isogenic pancreatic cell line and xenograft models expressing NRG1 fusions

We further assessed the activity of Zeno in pancreatic cells expressing NRG1 fusions. To this end, we introduced two *NRG1* fusions (*ATP1B1-NRG1* and *SLC3A2-NRG1*) into immortalized pancreatic ductal epithelial cells (H6c7). These cells can be transformed by introduction of oncogenes (8). We generated isogenic H6c7 cells stably expressing NRG1 fusions (Supplementary Fig. S2B, right panel) and then profiled them for activated signaling pathways using phospho-proteomic arrays (31). Expression of ATP1B1-NRG1 fusion in H6c7 cells resulted in increased phosphorylation of several proteins, including AKT and STAT3 (Fig. 2A-B), presumably via activation of HER3. Western blotting showed that treatment of H6c7-ATP1B1-NRG1 and H6c7-SLC3A2-NRG1 cells with Zeno resulted in a dose-dependent inhibition of phosphorylation of HER3 and AKT, with complete loss of phosphorylation at a concentration of just 1 nmol/L (Fig. 2C). Some differences between the cells expressing the two fusions were noted. For example, STAT3 and HER4 phosphorylation was inhibited to a higher degree by Zeno treatment in H6c7-ATP1B1-NRG1 cells compared to H6c7-SLC3A2-NRG1 cells. As observed with the breast cancer cell line with NRG1 fusion, phosphorylation of ERK1/2 remained largely unchanged with Zeno treatment (Fig. 2C-D). Treatment of the isogenic control H6c7-EV with Zeno decreased HER3 and HER2 phosphorylation at 100 nmol/L concentration without any substantial decrease in the other downstream signals examined (Supplementary Fig. S3C). Treatment of animals bearing H6c7-SLC3A2-NRG1 xenograft tumors with Zeno (25 mg/kg, once weekly) slowed tumor growth significantly (Supplementary Fig. S6A-B) without affecting animal weight (Supplementary Fig. S6C). We next examined the efficacy of Zeno in a pancreatic adenocarcinoma PDX model harboring an *APP-NRG1* fusion (CTG-0943). Treatment of mice bearing CTG-0943 PDX tumors with 2.5, 8 or 25 mg/kg Zeno once weekly resulted in a dose-dependent reduction in tumor growth (Fig. 2D). Area under curve (AUC) analysis showed that each of the three Zeno doses caused a significant reduction in tumor volume (Fig. 2E), with the 25 mg/kg QW dose being the most effective. Nine of the ten tumors in the 25 mg/kg QW group shrank by >50%, resulting in a $63 \pm 17\%$ decrease in tumor volume (Fig. 2F). These results support the data obtained with the H6c7-SLC3A2-NRG1 xenograft model, showing that Zeno therapy could be effective in pancreatic cancers driven by *NRG1* fusions.

Zeno is effective at blocking growth of lung and ovarian cancer PDX models at clinically relevant doses

The data above indicate that Zeno effectively inhibits growth and signals transduction in cell lines with *NRG1* alterations. We further analyzed the ability of Zeno to block the growth of NRG1 fusion-positive patient-derived xenograft (PDX) tumors from lung cancers (*CD74-NRG1* and *SLC3A2-NRG1*) and from a high-grade serous ovarian cancer (*CLU-NRG1*). Animals bearing established PDX tumors were treated once per week with Zeno (2.5, 8, or 25 mg/kg). Growth of the ST3204 model (lung cancer, *CD74-NRG1* fusion) was blocked at all doses of Zeno tested (Fig. 3A, left panel). AUC analysis showed all doses of Zeno caused a statistically significant reduction of growth, including tumor regression (Fig. 3A, middle panel). There was no difference between the three Zeno-treated groups, and tumor shrinkage was evident in all groups by the third day after treatment initiation. All

Zeno-treated ST3204 tumors shrank by 50–100% with the exception of one tumor in the 8 mg/kg group, which shrank initially by >50% but started to regrow towards the end of the study (Fig. 3A, right panel). There was one complete response (100% shrinkage). Treatment of a second lung cancer PDX model with a CD74-*NRG1* fusion (ST2891) resulted in a dose-dependent reduction in tumor volume (Supplementary Figure S6D). AUC analysis showed the reduction in tumor growth was statistically significant for the 8 mg/kg and 25 mg/kg groups, compared to vehicle-treated tumors (Supplementary Figure S6E). Two ST2891 tumors (one in the 8 mg/kg group and one in the 25 mg/kg group) shrank by 37% by the end of the study (Supplementary Figure S6F).

Administration of Zeno to mice implanted with LUAD-0061AS3 PDX tumors resulted in a dose-dependent reduction in tumor growth (Fig. 3B, left panel), and AUC analysis showed that tumor growth in all Zeno-treated groups was significantly lower than for vehicle-treated tumors (Fig. 3B, middle panel). In this model, tumor shrinkage was observed in the 8 and 25 mg/kg groups (Fig. 3B, right panel), and, as also observed in the ST3204 model, this was evident by the fourth day of treatment. Administration of Zeno was continued for 25 days after sacrifice of the animals in the vehicle arm (due to tumor size) to evaluate durability of the response to Zeno (Fig. 3B, right panel). Tumors in the 25 mg/kg group, a dose which results in similar steady-state serum concentrations as attained in the current human patient treatment regimen (750 mg every 2 weeks), remained significantly smaller than the average starting size (size before treatment (mean \pm SEM): $133.45 \pm 2.36 \text{ mm}^3$; size at study end: $88.85 \pm 5.78 \text{ mm}^3$). The best response in the two groups that showed tumor regression was 50% and 64% tumor shrinkage, respectively, for the 8 mg/kg and 25 mg/kg groups. Western blotting analysis of tumors extracted after Zeno treatment showed substantial reduction in HER and p70S6K phosphorylation, as well as downregulation of cyclin D1 and induced expression of cleaved PARP (Supplementary Fig. S6 G-H). These results suggest that Zeno treatment likely caused tumor regression by inhibiting the cell cycle and inducing apoptosis.

Expanding the histological groups of cancer with *NRG1* fusions that may benefit from Zeno therapy, we examined the efficacy of the antibody in a PDX model derived from a high-grade serous ovarian cancer (HGSOC). This PDX model (OV-10-0050) expresses a *CLU-NRG1* fusion and has previously been shown to respond to anti-HER2xHER3 therapy (24,26,27). Treatment of mice implanted with OV-10-0050 PDX tumors resulted in a dose-dependent reduction in growth (Fig. 3C, left panel). AUC analysis showed that tumor growth in all Zeno-treated groups was significantly lower than for vehicle-treated tumors (Fig. 3C, middle panel). Growth was reduced by $70.5 \pm 7.4\%$ in the 25 mg/kg group, and nine of ten tumors in this group shrank by $\geq 60\%$, with two complete regressions (Fig. 3C, right panel). Zeno treatment did not cause any reduction in animal weight in any of the studies (Supplementary Fig. S6C and Supplementary Fig. S7A-E) or any sign of ill health.

Clinical proof of efficacy in *NRG1* fusion-positive patients

Three patients with chemotherapy-resistant metastatic cancer were found to have *NRG1* fusion-positive tumors on genomic sequencing performed as part of routine care at Memorial Sloan Kettering Cancer Center (MSKCC). Zeno's promising activity in *NRG1* fusion-positive preclinical models, its previously established favorable toxicity profile in

patients with HER2+ breast and gastric cancer, and the absence of available clinical trials for this population at the time, led us to initiate Zeno treatment on single-patient protocols (26,28). All three patients experienced dramatic clinical and radiographic responses.

The first patient was a 50-year-old man who presented with stage IIB (pT3N1cM0) pancreatic ductal adenocarcinoma (PDAC). He underwent a pylorus-sparing pancreaticoduodenectomy (Fig 4A). DNA profiling of the tumor with MSK-IMPACT (32) revealed no *KRAS* mutation or other potential oncogenic driver (Supplementary Table S1). A postoperative CT scan showed no evidence of cancer, and he was treated with adjuvant chemotherapy consisting of gemcitabine and capecitabine. Unfortunately, his first scan four months into treatment demonstrated new liver metastases. Chemotherapy was changed to FOLFIRINOX (5-fluorouracil, leucovorin, irinotecan, and oxaliplatin). FOLFIRINOX was poorly tolerated as the patient experienced side effects including hypotension, hypertension, nausea, vomiting, and neuropathy. Thus, adjustments to treatment including dose reductions, split dosing, and omission of either irinotecan and/or oxaliplatin were made. He continued on chemotherapy for nine months, during which time his CA 19–9 (a tumor marker) levels continued to rise and CT scans revealed enlarging liver metastases. To further evaluate his tumor's genomics in the absence of a known *KRAS* mutation, RNA sequencing was performed on tissue from his primary resection using the MSK solid tumor fusion panel (33). This assay identified an in-frame fusion of *ATP1B1* exon 2 with *NRG1* exon 2. Given the *NRG1* gene fusion in his tumor, the lack of approved targeted therapy or appropriate clinical trials at that time for patients with this alteration, and the favorable activity foreseen with Zeno in this study, he then started Zeno on a single-patient protocol. Zeno was administered as an intravenous (IV) infusion, 750 mg every two weeks. Within weeks of treatment initiation, he achieved a clinical and pharmacodynamic response to therapy with improvement in his fatigue and anorexia, and a reduction in CA 19–9 levels from 262 to 56 U/mL. Imaging at eight weeks demonstrated a partial response (–44%) according to the Response Evaluation Criteria in Solid Tumors (RECIST) guidelines (version 1.1) and a complete response by PET response criteria (Fig. 4B) (34,35). His partial response continued with further tumor shrinkage to –82%, before ultimately progressing 14 months into treatment. Cell-free DNA (cfDNA) sequenced at the time of progression using a targeted NGS panel, MSK-ACCESS (36), demonstrated an emergent PTEN mutation (R233*). He continued on treatment for an additional five months for continued clinical benefit before being taken off therapy.

The second patient was a 34-year-old man who presented with PDAC metastatic to the liver. DNA-based sequencing determined his tumor was *KRAS* wild-type (Supplementary Table S1). He was treated with FOLFIRINOX for 14 months (Fig. 4C). Oxaliplatin was discontinued after cycle 11 due to neuropathy. He initially responded well to therapy, but ten months into treatment, when his chemotherapy was delayed for travel, he developed disease progression requiring an endoscopic retrograde cholangiopancreatography (ERCP) with biliary stent placement. A liver biopsy was performed, and RNA sequencing identified an in-frame fusion of *ATP1B1* exon 2 with *NRG1* exon 2. He was initiated on Zeno 750 mg IV every two weeks. He experienced rapid resolution of his tumor-associated abdominal pain and normalization of CA 19–9 levels (418 to 11 U/mL). Imaging at 6 weeks showed a tumor reduction of 22% that further decreased on subsequent imaging (–25%) (Fig. 4D). He

continued on treatment for 11 months before developing clinical disease progression with worsening abdominal and back pain. Profiling of cfDNA using MSK-ACCESS at the time of progression showed new CDKN2A H83D and TP53 G266* mutations.

The third patient was a 52-year-old man diagnosed with stage IIIB non-small cell lung cancer (NSCLC), mixed mucinous and non-mucinous adenocarcinoma. MSK-IMPACT profiling detected a fusion between *CD74* exon 7 and *NRG1* exon 6, and no other driver alterations in *EGFR*, *KRAS*, *ALK*, *ROS1*, *RET*, *BRAF*, *HER2*, *METex14*, or *NTRK* (Supplementary Table S1). He was treated with neoadjuvant cisplatin and pemetrexed followed by a left lower lobectomy (LLL), left upper lobe (LUL) wedge resection, mediastinal and regional lymphadenectomy, and post-operative radiation (Fig. 4E). The first post-treatment CT scan showed new lung metastases. He was initiated on afatinib to target the *NRG1* fusion, but developed rapid clinical and radiological disease progression including new brain and lung metastases. He was subsequently treated with carboplatin, pemetrexed, and pembrolizumab for four cycles, followed by pemetrexed/pembrolizumab maintenance with stable disease lasting five months before radiographic progression. He went on to receive three additional lines of systemic therapy and two rounds of stereotactic radiosurgery (SRS) to the brain. Unfortunately, his disease was chemo-refractory and he progressed through each line of chemotherapy. In an attempt to target the *NRG1* fusion identified in his tumor, he was started on Zeno under a single-patient protocol, 750 mg IV every two weeks. He responded rapidly to treatment, with scans showing a partial response (−33%) by RECIST v1.1 at eight weeks, and tumor shrinkage in the brain (Fig. 4F). His response further deepened at 4 months (−41%) with improvement in his chronic dizziness. Five months into treatment he became pancytopenic. A bone marrow biopsy confirmed myelodysplastic syndrome with excess blasts (MDS-EB1), which was believed to be related to his prior chemotherapy and radiation treatments, and unrelated to Zeno. In this setting, Zeno was held and he developed worsening MDS and progressive lung cancer. Zeno was briefly restarted given the prior clinical benefit; however, he experienced a rapid clinical decline with refractory cytopenias and development of hemorrhagic metastases. He was placed in hospice care and died shortly thereafter.

Discussion

Solid tumors driven by *NRG1* fusions comprise a molecularly defined subset of cancer for which there is no approved therapy targeting the driver genomic alteration. Here we examined the efficacy of targeting HER3, the predominant receptor for oncogenic *NRG1* fusions, through a unique “dock and block” mechanism using Zeno, a HER2xHER3 bispecific antibody (26). Treatment of *NRG1* fusion-positive cell lines and/or patient-derived xenograft models generated from lung, breast, ovarian, and pancreatic cancers with Zeno at or below clinically relevant doses resulted in reduced cell growth, induction of apoptosis, and tumor shrinkage in some PDX models. Mechanistic studies demonstrated that Zeno potently decreased phosphorylation of HER2, HER3, EGFR, and HER4, and reduced transmission of *NRG1* fusion-dependent signaling via growth and survival pathways such as AKT, mTOR, and STAT. Notably, the MEK-ERK pathway was less responsive to Zeno treatment in three of the five cell lines with *NRG1* fusions that we tested. Suppression of *NRG1* fusion-dependent signaling resulted in loss of expression of the cell cycle activator

cyclin D1 and increased expression of cell cycle inhibitors (P21 and P27), in addition to increased expression of the pro-apoptotic proteins BIM, cleaved PARP and PUMA. Taken together, these results demonstrate that Zeno inhibits growth of tumors driven by *NRG1* rearrangements by blocking downstream signaling, reducing entry into the cell cycle, and inducing cell death. The efficacy of Zeno in *NRG1* fusion-positive cell lines but not isogenic non-fusion counterparts suggests that *NRG1* alterations confer oncogene addiction. To our knowledge, *NRG1* is the first oncogenic genomically altered receptor ligand, and cancers with *NRG1* fusions are the first malignancies arising from fusion proteins to be effectively targeted with antibody therapy.

While Zeno treatment lowered HER2 and HER3 phosphorylation in isogenic control HBEC and H6c7 cell lines, this did not translate into substantial inhibition of downstream signaling. This contrasts with the isogenic counterparts expressing *NRG1* fusions. These results further show that expression of *NRG1* fusions co-opt downstream growth and survival pathways to drive tumorigenesis. Although we observed differential sensitivity of cell lines to Zeno, we are unable to see any causal relationship between the tissue of origin of the cell lines or the fusion partner and sensitivity to Zeno. Similarly, we noted varying sensitivity of PDX models to Zeno. The LUAD-0061AS3 PDX model with an *SLC3A2-NRG1* fusion and the ST3204 model with a *CD74-NRG1* fusion responded very well to Zeno therapy, with all tumors shrinking >50% with the 25 mg/kg QW dose. However, data obtained with the ST2891 PDX model, which also harbors a *CD74-NRG1* fusion, showed that only one tumor in the group showed tumor regression. The limited number of models and fusions prevents us from making conclusions as to whether any histology or tumor with a particular fusion partner is more likely to respond to Zeno.

Given the mechanistic and preclinical data, Zeno was tested in three patients with chemotherapy-resistant *NRG1* fusion-positive metastatic cancer prior to the availability of a clinical trial, all of whom experienced unequivocal clinical benefit. Two patients with *ATP1B1-NRG1* fusion-positive pancreatic cancer experienced tumor shrinkage, resolution of disease-related symptoms, and profound improvement in quality of life. They continued on therapy with minimal toxicity for 19 and 11 months. This is especially remarkable given the unmet need in pancreatic cancer, with more than half of patients dying within a year of treatment initiation (37). There are currently no approved therapies after first and second-line chemotherapy, and patients are typically treated with supportive care or enrolled in a clinical trial. Targeted therapy trials for pancreatic cancer have previously focused on the use of monoclonal antibodies and kinase inhibitors targeting primarily EGFR, VEGF, or KRAS without significant benefit, even when combined with systemic chemotherapy (38,39). More recently, the observation that 4–7% of patients with pancreatic cancer harbor germline *BRCA* (*gBRCA*) mutations has led to clinical trials targeting DNA repair pathways and the approval of olaparib as maintenance therapy after chemotherapy in this population (40). While *gBRCA* mutations occur in the minority of patients with pancreatic cancer, the validation of a genomic biomarker in this population is likely to increase the rate of both germline and somatic testing, thus identifying patients with *NRG1* fusions. Importantly, *NRG1* rearrangements are often not detected by DNA-based sequencing techniques due to the large introns in *NRG1* that are not typically included in targeted panels or whole-exome sequencing. RNA-based sequencing is a superior method for identifying these alterations

and should be performed in patients with *KRAS* wild-type pancreatic cancer to look more comprehensively for *NRG1* fusions.

The third patient, a man with otherwise driver-negative NSCLC, experienced a partial response and disease control in the brain for several months before unfortunately developing unrelated clinical decompensation. Despite having rapidly progressed through six lines of prior systemic therapy, including afatinib, he had brisk tumor shrinkage on Zeno. Interestingly, his lack of response to prior therapy may reflect a more universal tendency for *NRG1* fusion-positive NSCLC to have poor prognostic features and respond poorly to standard chemoimmunotherapy (41). Moreover, *NRG1* rearrangements are typically mutually exclusive with alterations in other drivers in lung cancer such as *EGFR*, *KRAS*, *ALK*, *ROS1*, *RET*, and *NTRK*, further limiting treatment options (1). Therefore, while many therapies exist for lung cancer, patients with tumors driven by *NRG1* fusions are still in desperate need of better therapy.

Zeno is an ADCC-enhanced anti-HER2×HER3 bispecific antibody that ‘docks’ on HER2 to optimally position the antibody to bind HER3 and subsequently ‘block’ NRG1 from interacting with HER3, effectively preventing HER2:HER3 heterodimerization and downstream signaling (26). This unique mechanism of action seems optimally suited for treating patients with NRG1 fusion-positive cancer. Although clinical responses to other HER2 and/or HER3-targeted therapy have been reported in patients harboring NRG1 fusions, it is not possible to determine response rates or compare therapies due to the anecdotal nature of these reports, the general bias towards publishing positive results, and the heterogeneity of the methods used to assess clinical benefit outside of a clinical trial setting. Similarly, a notable drawback of our report is the small number of patients described, limited by the number of patients treated on single patient protocols at MSK. We expect to better understand the efficacy of Zeno when results from a larger multi-institutional clinical trial are published.

We previously reported a durable partial response lasting 19 months in a NSCLC patient treated with the anti-HER3 antibody therapy GSK2849330 (24). In a published report summarizing 19 cases treated with afatinib, seven cases showed partial responses lasting from 3 to 12 months and three cases lasting 18 to 27 months (25). Five cases showed stable or progressive disease. Notably, the toxicity with afatinib is significant and may be particularly challenging in the *NRG1* fusion-positive population. In a phase III study of afatinib vs. cisplatin in *EGFR*-mutant lung cancer, more than half of patients (52%) required dose reductions for toxicity, and 95% had treatment-related diarrhea, including 14% with grade 3 diarrhea (42). The high likelihood for drug-induced diarrhea is especially concerning when treating patients with pancreatic cancer who often have some degree of pancreatic insufficiency leading to chronic diarrhea. This is in stark contrast with Zeno, which is well tolerated, with treatment-related diarrhea seen in only 20% of patients (the most common related adverse event), all grade 1 or 2 (41). As a comparison, 66% of patients treated with GSK2849330 in a phase 1 trial had treatment-related diarrhea (43).

There has been no published direct comparison of Zeno with other potential anti-HER therapy such as afatinib, seribantumab or GSK2849330 in NRG1-fusion patient-derived

xenograft models. Comparing previously published studies in the LUAD-0061AS3 PDX model (29) and the current study, Zeno (25 mg/kg QW) was more effective than GSK2849330 (25 mg/kg BIW) at causing tumor regression. Seribantumab was as effective as Zeno at inhibiting growth of LUAD-0061AS3 PDX tumors. In the OV-10–0050 ovarian cancer model, GSK2849330 and seribantumab (all PDX tumors shrank by 100%) was more effective than Zeno at different doses used (24,27). However, caution should be exercised in interpreting these preclinical data as none of these potential therapeutic agents were compared in the same study.

In summary, the data presented in this study underscore the treatment potential for Zeno, an anti-HER2xHER3 bispecific antibody, as a new treatment specifically targeting *NRG1* fusion-positive cancers. Zeno binds to, and blocks HER3 from interacting with NRG1 or the NRG1 fusion protein. This inhibition leads to potent efficacy in preclinical models and durable responses in patients who have few, if any, therapeutic options. Zeno is a promising therapeutic option in development for patients with NRG1 fusion-positive cancers. Based on this proof-of-concept, a global, multicenter phase 1/2 clinical trial for *NRG1* fusion-positive cancers has been initiated (eNRGy trial, [NCT02912949](https://clinicaltrials.gov/ct2/show/study/NCT02912949)).

Materials and Methods

A list of antibodies used in this study is provided in Supplementary Table S2.

Cell lines and PDX models.

The breast cancer epithelial cell lines MDA-MB-175-VII (Cat# HTB-25, RRID: CVCL_1400) and MCF-7 (Cat# HTB-22, RRID: CVCL_0031) were obtained from the American Type Culture Collection (ATCC, Manassas, VA). MDA-MB-175-VII cells express a *DOC4-NRG1* fusion (12,24). MCF-7 cells were derived from pleural effusion isolated from a patient with breast cancer and are ER positive (44). This cell line has been profiled by the Broad Institute DepMap program and does not have any *NRG1* rearrangement (45). Human bronchial epithelial cells were immortalized by overexpression of CDK4 and TERT (HBEC-3KT cell line) and were obtained from Dr. John Minna (UT South Western, TX, USA) (46). A p53 C-terminal mutant was introduced into HBEC-3KT (HBECp53) as described previously (47) and a CD74-NRG1 or VAMP2-NRG1 (custom synthesized by GeneCopoeia, Rockville, MD) fusion was expressed in these cells by lentiviral-mediated transduction of the cDNAs. Stable cell lines were selected with 200 µg/mL hygromycin. The immortalized pancreatic ductal epithelial cell line H6c7 (CVCL_0P38) (48) was purchased from Kerfast (Boston, MA). The *DOC4-NRG1*, *ATP1B1-NRG1* and *SLC3A2-NRG1* fusions were amplified by PCR from MDA-MB-175-VII cells, a pancreatic adenocarcinoma sample and LUAD-0061AS3 cells, respectively, and then cloned into the retroviral pCX4 vector. Cells were transduced with PCX4-empty plasmid or PCX4-NRG1 fusion plasmids. Cells expressing the empty plasmid or fusion were selected using 750 µg/mL bleomycin. HCC-95 cells were obtained from Dr. William Lockwood (BC Cancer Center, Vancouver, BC, Canada, RRID: CVCL_5137), and these cells were found to have *NRG1* amplification by whole exome sequencing (24). The LUAD-0061AS3 PDX model was generated from a sample obtained from a patient with *SLC3A2-NRG1* fusion-driven lung cancer. The

patient exhibited disease progression while on treatment with afatinib (40 mg/day) at the time of collection of the sample used to generate the model as described previously (29). The LUAD-0061AS3 cell line was generated from LUAD-0061AS3 PDX tumor tissue obtained after seven serial passages (29). Cell lines were tested for mycoplasma every 3–6 months (MycoAlert kit, Lonza) with the most recent testing conducted three months prior to completion of the studies in this manuscript. Authenticated cell lines purchased from ATCC one year prior to the studies were expanded and stocks were frozen. A new vial of cells was thawed and used for 10–15 passages (every two months) and the known oncogene was verified by RT-PCR each time. The identity of models that were created in our laboratory was confirmed by MSK-IMPACT profiling, and this was routinely confirmed by testing for the known oncogene fusion. The ST3204 and ST2891 lung cancer PDX models were genomically characterized by RNA sequencing and the *CD74-NRG1* fusion was confirmed by XenoStart (San Antonio, Tx). The CTG-0943 pancreatic adenocarcinoma PDX model was genomically characterized by RNA sequencing and the *APP-NRG1* fusion confirmed by Champions Oncology (Rockville, MD). The OV-10–0050 PDX model was characterized by RNA sequencing and the *CLU-NRG1* fusion confirmed by PCR (27).

Growth and propagation of cell lines.

The MDA-MB-175-VII cell line was maintained in DMEM: Ham's F12 (1:1) medium supplemented with 20% FBS. For experiments, MDA-MB-175-VII cells were plated and grown in DMEM: Ham's F12 medium containing 10% FBS. MCF-7 cells were grown in DMEM supplemented with 10% FBS. HBECp53 cells were grown in KSM supplemented with bovine pituitary extract and EGF. Isogenic HBECp53 cell lines expressing *NRG1* fusions were grown in DMEM: Ham's F12 (1:1) medium supplemented with 10% FBS. HCC-95 cells were grown in RPMI-1640 supplemented with 10% FBS. All growth media were supplemented with 1% antibiotic (penicillin/streptomycin mixture). Cells were subcultured using trypsin (0.25%)/EDTA (1 mM) when stock flasks reached 75% confluency and re-plated at a 1:3 dilution. Cells were kept in a humidified incubator infused with 5% CO₂ and maintained at 37°C.

Growth and apoptosis assays.

For dose-response studies, cells were plated at a density of 3,500 cells in white clear-bottom 96-well plates in a volume of 100 µL complete growth medium. Twenty four hours later, the growth media were replaced with 180 µL serum-free media as described previously and 20 µL inhibitors added at 10X concentration (to achieve 1X concentration) in a final volume of 200 µL. After 96 h incubation, 20 µL alamarBlue cell viability reagent was added to achieve a final concentration of 10%. AlamarBlue is a cell-permeable pH-sensitive dye that is reduced when it enters the mitochondria and emits fluorescence at a different wavelength. Fluorescence was measured (Ex: 530 nm, Em: 585 nm) using a Molecular Dynamics Spectramax M2 fluorescence plate reader. In each experiment, background fluorescence was determined in cells treated with 1 µM of the 20S proteasome inhibitor carfilzomib, which is toxic to most cells at high concentrations, and this background was subtracted from all values. There were 3–4 replicates of each condition. Relative IC₅₀ and 95% CI values were determined by non-linear regression analysis using GraphPad Prism 8 software using either a variable slope model or, in cases where inhibition was only partial, a three-parameter

fit. The curve fitting resulted in $R^2 > 0.8$ for the data sets. Each condition was assayed in triplicate in at least two independent experiments. Caspase 3/7 enzymatic activity was measured using a fluorescence-based assay as previously described (27).

Efficacy studies in animals.

Animal care and experiments were conducted in accordance with a protocol approved by the Memorial Sloan Kettering Cancer Center Institutional Animal Care and Use Committee and Research Animal Resource Center and in accordance with Institutional Animal Care and Use Committee approved protocols at XenoSTART and Champions Oncology). Crushed PDX tumor samples were mixed with matrigel (50%) and injected into the subcutaneous flank of 6 to 12-week-old female NSGTM (LUAD-0061AS3), BALB/c nude (OV-10-0050) or athymic nude (ST2891, ST3204 and CTG-0953) mice. When tumors reached approximately 125–250 mm³, mice were randomized to groups of 5–10 and treatment commenced. Zeno was administered in phosphate-buffered saline by injection into the peritoneal cavity once per week. Mice were observed daily throughout the treatment period for signs of morbidity and mortality. Tumor length and width, and animal weights were measured twice weekly. Tumor volume was calculated using the empirical formula $V = \text{length} \times \text{width}^2 \times 0.52$. The percent change in each tumor volume was calculated using the formula $((V2-V1)/V1) \times 100$, where V1 is the starting tumor volume and V2 is the final tumor volume.

Preparation of whole-cell extracts and western blotting.

Cells were lysed in 1X RIPA lysis buffer supplemented with phosphatase and protease inhibitors. The whole-cell extracts were then denatured in 2X Laemmli sample buffer at 55°C for 15 min, resolved on 4–12% NuPAGE gels (Invitrogen) and transferred onto polyvinylidene fluoride (PVDF) membranes. Membranes were blocked in 3% bovine serum albumin in tris-buffered saline supplemented with 0.1% Tween-20 (vol/vol) for 1 h at room temperature and probed with primary antibodies (see Supplementary Table S2 for complete list of antibodies and specificity). Bound antibodies were detected with peroxidase-labeled goat secondary antibody raised against mouse or rabbit IgG (R&D Systems, Minneapolis, MN) and imaged with enhanced chemiluminescence (ECL) western blotting detection reagent (GE Healthcare). Images were captured on x-ray films. Western blotting was conducted at least two times from independently prepared samples.

Proteome profiling arrays.

We used a human proteome profiling array system (R&D Systems) that contains duplicate validated positive and negative controls and capture antibodies that can simultaneously detect the phosphorylation state of 43 human kinases (Proteome Profiler Human Phosphokinase Array kit; for coordinate annotation see www.rndsystems.com) (31). Five million cells were plated in 10-cm dishes and grown for 48 h. Cells were deprived of serum by culturing for 24 h in growth media supplemented with 0.05% FBS. Whole-cell extracts were then prepared, and detection of protein phosphorylation was carried out according to the manufacturer's instructions. In brief, the array membranes were blocked, incubated with 350 µg total cellular protein per array overnight at 4 °C on a rocking platform, washed, and incubated with phospho-specific detection antibodies. Captured phosphorylated proteins

were detected by ECL and imaged on x-ray films. The average pixel densities of duplicate spots were measured using ImageJ software and are expressed relative to the positive control on each array.

⁵¹Chromium release assays.

Antibody-dependent cell-mediated cytotoxicity (ADCC) was assessed using a ⁵¹Cr release assay. Briefly, tumor cells were labeled with sodium ⁵¹Cr chromate (Amersham, Arlington Height, IL) at 100 mCi/10⁶ cells at 37°C for 1 h. After two washes, tumor cells were plated in a 96-well plate before mixing with human peripheral mononuclear cells with various concentrations of Zeno, trastuzumab, or non-specific IgG1. Cytotoxicity was analyzed after incubation at 37°C for 4 h. The released ⁵¹Cr was measured by a gamma counter (Packed Instrument, Downers Grove, IL). Percentage of specific lysis was calculated using the formula: 100% x (experimental cpm—background cpm)/(total cpm—background cpm), where cpm represent counts per minute of ⁵¹Cr released. Total release of ⁵¹Cr was assessed by lysis with 10% SDS, and background release was measured in the absence of effector cells and antibodies.

Molecular diagnostics, patients and treatments.

The single-patient protocols were approved by the MSKCC Institutional Review Board. Written informed consent was obtained from patients and the study was conducted in accordance with the guidelines of the Declaration of Helsinki. All patient samples were profiled using our center's Integrated Mutation Profiling of Actionable Cancer Targets platform (MSK-IMPACT), which is a large-panel next-generation sequencing (NGS) assay designed to detect mutations, copy-number alterations, and selected fusions involving up to 505 cancer-associated genes (32). Two patients were also profiled using an RNA-based solid tumor fusion-panel assay (MSK-Fusion) (33). Patients with *NRG1* fusion-positive tumors were treated with Zeno (750 mg intravenously, every 2 weeks) on FDA-approved single-patient protocols. Response to therapy was assessed by CT scans using RECIST v1.1 criteria (35).

Statistical analysis.

Tumor data sets were compared by two-way ANOVA, with Dunnett's or Tukey's multiple comparison test to determine significance. *P*<0.05 was considered a statistically significant difference between two values or data sets. Area under curve (AUC) analysis was calculated by the trapezoid rule and groups were compared using one-way ANOVA with two-tailed Student's t-test. All statistical analysis was conducted using GraphPad Prism 8 software (RRID: SCR_002798). All experiments consisted of 2–6 replicates per condition, and data is expressed as mean ± SD or SEM as indicated in figure legends.

Supplementary Material

Refer to Web version on PubMed Central for supplementary material.

Financial Support:

Financial support for this study was provided by a grant from Cycle for Survival to M. Ladanyi; a grant from the National Institute of Health to E. de Stanchina (U54 OD020355); a Memorial Sloan Kettering Cancer Center Support Grant (P30 CA008748); funding from Merus N.V to R. Somwar and M. Ladanyi; and by ASCO's Conquer Cancer Foundation Career Development Award to A. Schram.

Conflict of Interest Disclosure:

Igor Odintsov, Madelyn Espinosa-Cotton, Inna Khodos, Marissa S. Mattar, Allan J.W. Lui, Whitney J. Sisso, Morana Vojnic and Elisa de Stanchina report no potential conflict of interest.

Alison M. Schram has received advisory board compensation from Relay Therapeutics and research funding paid to institution from AstraZeneca, ArQule, BeiGene, Black Diamond Therapeutics, Kura, Lilly, Merus, Northern Biologics, Pfizer, Relay, and Surface Oncology.

Marie N. O'Connor, Cecile A.W. Geuijen, Ron C. J. Schackmann, Jeroen J. Lammerts van Bueren and Ernesto Wasserman are employees of, and hold stock options and/or shares in Merus N.V.

Jean Torrisi is a consultant for Eli Lilly Loxo Oncology.

Eileen O'Reilly has received advisory board/consulting compensation from Cytomx Therapeutics (DSMB), Rafael Therapeutics (DSMB), Sobi, Silenseed, Tyme, Seagen, Molecular Templates, Boehringer Ingelheim, BioNTech, Ipsen, Polaris, Merck, IDEAYA, Cend, AstraZeneca, Noxxon, BioSapien, Cend Therapeutics, Bayer (spouse), Genentech-Roche (spouse), Celgene-BMS (spouse), Eisai (spouse); and research funding paid to institution from Genentech/Roche, Celgene/BMS, BioNTech, AstraZeneca, Arcus, Elicio, Parker Institute, AstraZeneca.

Marc Ladanyi has received advisory board compensation from Merck, Bristol-Myers Squibb, Takeda, Bayer, Lilly Oncology, Janssen, and Paige.AI. In addition, he has received research support from LOXO Oncology, Helsinn Healthcare, Elevation Oncology Inc. unrelated to the current submission. Research funding from Merus N.V. partially supported this study.

Alex Drilon has received advisory board compensation from Ignyta/Genentech/Roche, Loxo/Bayer/Lilly, Takeda/Ariad/Millennium, TP Therapeutics, AstraZeneca, Pfizer, Blueprint Medicines, Helsinn, Beigene, BergenBio, Hengrui Therapeutics, Exelixis, Tyra Biosciences, Verastem, MORE Health, Abbvie, 14ner/Elevation Oncology, Remedica Ltd., ArcherDX, Monopteros, Novartis, EMD Serono, Melendi, Liberum, Repare RX, Nuvalent, Merus, AXIS, Chugai Pharm, EPG Health; research funding paid to institution from Pfizer, Exelixis, GlaxoSmithKlein, Teva, Taiho, PharmaMar; Royalties from Wolters Kluwer; Other: Merck, Puma, Merus, Boehringer Ingelheim

Rommel Somwar has received research support from Helsinn Healthcare, LOXO Oncology, Merus, and Elevation Oncology Inc, unrelated to the current submission. Research funding from Merus N.V. partially supported this study.

Data availability statement.

Data generated in this study are available upon request from the corresponding authors.

REFERENCES

1. Jonna S, Feldman RA, Swensen J, Gatalica Z, Korn WM, Borghaei H, et al. Detection of NRG1 Gene Fusions in Solid Tumors. *Clin Cancer Res* 2019;25(16):4966–72 doi 10.1158/1078-0432.CCR-19-0160. [PubMed: 30988082]
2. Ptakova N, Martinek P, Holubec L, Janovsky V, Vancurova J, Grossmann P, et al. Identification of tumors with NRG1 rearrangement, including a novel putative pathogenic UNC5D-NRG1 gene fusion in prostate cancer by data-drilling a de-identified tumor database. *Genes Chromosomes Cancer* 2021;60(7):474–81 doi 10.1002/gcc.22942. [PubMed: 33583086]
3. Huang HE, Chin SF, Ginestier C, Bardou VJ, Adelaide J, Iyer NG, et al. A recurrent chromosome breakpoint in breast cancer at the NRG1/neuregulin 1/hereregulin gene. *Cancer Res* 2004;64(19):6840–4 doi 10.1158/0008-5472.CAN-04-1762. [PubMed: 15466169]

4. Fernandez-Cuesta L, Plenker D, Osada H, Sun R, Menon R, Leenders F, et al. CD74-NRG1 fusions in lung adenocarcinoma. *Cancer Discov* 2014;4(4):415–22 doi 10.1158/2159-8290.CD-13-0633. [PubMed: 24469108]
5. Dhanasekaran SM, Balbin OA, Chen G, Nadal E, Kalyana-Sundaram S, Pan J, et al. Transcriptome meta-analysis of lung cancer reveals recurrent aberrations in NRG1 and Hippo pathway genes. *Nat Commun* 2014;5:5893 doi 10.1038/ncomms6893. [PubMed: 25531467]
6. Nakaoku T, Tsuta K, Ichikawa H, Shiraishi K, Sakamoto H, Enari M, et al. Druggable oncogene fusions in invasive mucinous lung adenocarcinoma. *Clin Cancer Res* 2014;20(12):3087–93 doi 10.1158/1078-0432.CCR-14-0107. [PubMed: 24727320]
7. Heining C, Horak P, Uhrig S, Codo PL, Klink B, Hutter B, et al. NRG1 Fusions in KRAS Wild-Type Pancreatic Cancer. *Cancer Discov* 2018;8(9):1087–95 doi 10.1158/2159-8290.CD-18-0036. [PubMed: 29802158]
8. Jones MR, Williamson LM, Topham JT, Lee MKC, Goytain A, Ho J, et al. NRG1 Gene Fusions Are Recurrent, Clinically Actionable Gene Rearrangements in KRAS Wild-Type Pancreatic Ductal Adenocarcinoma. *Clin Cancer Res* 2019;25(15):4674–81 doi 10.1158/1078-0432.CCR-19-0191. [PubMed: 31068372]
9. Duruisseaux M, McLeer-Florin A, Antoine M, Alavizadeh S, Poulot V, Lacave R, et al. NRG1 fusion in a French cohort of invasive mucinous lung adenocarcinoma. *Cancer Med* 2016;5(12):3579–85 doi 10.1002/cam4.838. [PubMed: 27770508]
10. Laskin J, Liu SV, Tolba K, Heining C, Schlenk RF, Cheema P, et al. NRG1 fusion-driven tumors: biology, detection, and the therapeutic role of afatinib and other ErbB-targeting agents. *Ann Oncol* 2020;31(12):1693–703 doi 10.1016/j.annonc.2020.08.2335. [PubMed: 32916265]
11. Bernardino J, Apiou F, Gerbault-Seureau M, Malfroy B, Dutrillaux B. Characterization of recurrent homogeneously staining regions in 72 breast carcinomas. *Genes Chromosomes Cancer* 1998;23(2):100–8 doi 10.1002/(sici)1098-2264(199810)23:2<100::aid-gcc2>3.0.co;2-6. [PubMed: 9739012]
12. Wang XZ, Jolicoeur EM, Conte N, Chaffanet M, Zhang Y, Mozziconacci MJ, et al. gamma-hereregulin is the product of a chromosomal translocation fusing the DOC4 and HGL/NRG1 genes in the MDA-MB-175 breast cancer cell line. *Oncogene* 1999;18(41):5718–21 doi 10.1038/sj.onc.1202950. [PubMed: 10523851]
13. Liu X, Baker E, Eyre HJ, Sutherland GR, Zhou M. Gamma-hereregulin: a fusion gene of DOC-4 and neuregulin-1 derived from a chromosome translocation. *Oncogene* 1999;18(50):7110–4 doi 10.1038/sj.onc.1203136. [PubMed: 10597312]
14. Shin DH, Lee D, Hong DW, Hong SH, Hwang JA, Lee BI, et al. Oncogenic function and clinical implications of SLC3A2-NRG1 fusion in invasive mucinous adenocarcinoma of the lung. *Oncotarget* 2016;7(43):69450–65 doi 10.18632/oncotarget.11913. [PubMed: 27626312]
15. Weinstein EJ, Leder P. The extracellular region of heregulin is sufficient to promote mammary gland proliferation and tumorigenesis but not apoptosis. *Cancer Res* 2000;60(14):3856–61. [PubMed: 10919660]
16. Roskoski R Jr., The ErbB/HER receptor protein-tyrosine kinases and cancer. *Biochem Biophys Res Commun* 2004;319(1):1–11. [PubMed: 15158434]
17. Wang Z. ErbB Receptors and Cancer. *Methods Mol Biol* 2017;1652:3–35 doi 10.1007/978-1-4939-7219-7_1. [PubMed: 28791631]
18. Tzahar E, Levkowitz G, Karunagaran D, Yi L, Peles E, Lavi S, et al. ErbB-3 and ErbB-4 function as the respective low and high affinity receptors of all Neu differentiation factor/hereregulin isoforms. *J Biol Chem* 1994;269(40):25226–33. [PubMed: 7929212]
19. Yarden Y, Sliwkowski MX. Untangling the ErbB signalling network. *Nat Rev Mol Cell Biol* 2001;2(2):127–37. [PubMed: 11252954]
20. Zhang X, Gureasko J, Shen K, Cole PA, Kuriyan J. An allosteric mechanism for activation of the kinase domain of epidermal growth factor receptor. *Cell* 2006;125(6):1137–49 doi 10.1016/j.cell.2006.05.013. [PubMed: 16777603]
21. van Lengerich B, Agnew C, Puchner EM, Huang B, Jura N. EGF and NRG induce phosphorylation of HER3/ERBB3 by EGFR using distinct oligomeric mechanisms. *Proc Natl Acad Sci U S A* 2017;114(14):E2836–E45 doi 10.1073/pnas.1617994114. [PubMed: 28320942]

22. Chen CH, Chernis GA, Hoang VQ, Landgraf R. Inhibition of heregulin signaling by an aptamer that preferentially binds to the oligomeric form of human epidermal growth factor receptor-3. *Proc Natl Acad Sci U S A* 2003;100(16):9226–31 doi 10.1073/pnas.1332660100. [PubMed: 12874383]
23. Klapper LN, Glathe S, Vaisman N, Hynes NE, Andrews GC, Sela M, et al. The ErbB-2/HER2 oncoprotein of human carcinomas may function solely as a shared coreceptor for multiple stroma-derived growth factors. *Proc Natl Acad Sci U S A* 1999;96(9):4995–5000 doi 10.1073/pnas.96.9.4995. [PubMed: 10220407]
24. Drilon A, Somwar R, Mangatt BP, Edgren H, Desmeules P, Ruusulehto A, et al. Response to ERBB3-Directed Targeted Therapy in NRG1-Rearranged Cancers. *Cancer Discov* 2018;8(6):686–95 doi 10.1158/2159-8290.CD-17-1004. [PubMed: 29610121]
25. Cadranel J, Liu SV, Duruisseaux M, Branden E, Goto Y, Weinberg BA, et al. Therapeutic Potential of Afatinib in NRG1 Fusion-Driven Solid Tumors: A Case Series. *Oncologist* 2021;26(1):7–16 doi 10.1634/theoncologist.2020-0379. [PubMed: 32852072]
26. Geuijen CAW, De Nardis C, Maussang D, Rovers E, Gallenne T, Hendriks LJA, et al. Unbiased Combinatorial Screening Identifies a Bispecific IgG1 that Potently Inhibits HER3 Signaling via HER2-Guided Ligand Blockade. *Cancer Cell* 2018;33(5):922–36 e10 doi 10.1016/j.ccell.2018.04.003. [PubMed: 29763625]
27. Odintsov I, Lui AJW, Sisso WJ, Gladstone E, Liu Z, Delasos L, et al. The Anti-HER3 mAb Seribantumab Effectively Inhibits Growth of Patient-Derived and Isogenic Cell Line and Xenograft Models with Oncogenic NRG1 Fusions. *Clin Cancer Res* 2021;27(11):3154–66 doi 10.1158/1078-0432.CCR-20-3605. [PubMed: 33824166]
28. Alsina M, Boni V, Schellens JHM, Moreon V, Bol K, Westendorp M, et al. First-in-human phase 1/2 study of MCLA-128, a full length IgG1 bispecific antibody targeting HER2 and HER3: Final phase 1 data and preliminary activity in HER2+ metastatic breast cancer (MBC). *Journal of Clinical Oncology* 2017;35(15 suppl):1 doi 10.1200/JCO.2017.35.15_suppl.2522 [PubMed: 28034063]
29. Odintsov I, Mattar MS, Lui AJW, Offin M, Kurzatkowski C, Delasos L, et al. Novel Preclinical Patient-Derived Lung Cancer Models Reveal Inhibition of HER3 and MTOR Signaling as Therapeutic Strategies for NRG1 Fusion-Positive Cancers. *J Thorac Oncol* 2021;16(7):1149–65 doi 10.1016/j.jtho.2021.03.013. [PubMed: 33839363]
30. Howarth KD, Mirza T, Cooke SL, Chin SF, Pole JC, Turro E, et al. NRG1 fusions in breast cancer. *Breast Cancer Res* 2021;23(1):3 doi 10.1186/s13058-020-01377-5. [PubMed: 33413557]
31. Hayashi T, Odintsov I, Smith RS, Ishizawa K, Liu AJW, Delasos L, et al. RET inhibition in novel patient-derived models of RET-fusion positive lung adenocarcinoma reveals a role for MYC upregulation. *Dis Model Mech* 2020;14(2):dmm047779 doi 10.1242/dmm.047779.
32. Cheng DT, Mitchell TN, Zehir A, Shah RH, Benayed R, Syed A, et al. Memorial Sloan Kettering-Integrated Mutation Profiling of Actionable Cancer Targets (MSK-IMPACT): A Hybridization Capture-Based Next-Generation Sequencing Clinical Assay for Solid Tumor Molecular Oncology. *J Mol Diagn* 2015;17(3):251–64 doi 10.1016/j.jmoldx.2014.12.006.
33. Benayed R, Offin M, Mullaney K, Sukhadia P, Rios K, Desmeules P, et al. High Yield of RNA Sequencing for Targetable Kinase Fusions in Lung Adenocarcinomas with No Mitogenic Driver Alteration Detected by DNA Sequencing and Low Tumor Mutation Burden. *Clin Cancer Res* 2019;25(15):4712–22 doi 10.1158/1078-0432.CCR-19-0225. [PubMed: 31028088]
34. Ulaner GA, Saura C, Piha-Paul SA, Mayer I, Quinn D, Jhaveri K, et al. Impact of FDG PET Imaging for Expanding Patient Eligibility and Measuring Treatment Response in a Genome-Driven Basket Trial of the Pan-HER Kinase Inhibitor, Neratinib. *Clin Cancer Res* 2019;25(24):7381–7 doi 10.1158/1078-0432.CCR-19-1658. [PubMed: 31548342]
35. Eisenhauer EA, Therasse P, Bogaerts J, Schwartz LH, Sargent D, Ford R, et al. New response evaluation criteria in solid tumours: revised RECIST guideline (version 1.1). *Eur J Cancer* 2009;45(2):228–47 doi 10.1016/j.ejca.2008.10.026. [PubMed: 19097774]
36. Brannon AR, Jayakumaran G, Diosdado M, Patel J, Razumova A, Yu Hu, et al. Enhanced specificity of clinical high-sensitivity tumor mutation profiling in cell-free DNA via paired normal sequencing using MSK-ACCESS. *Nature Communications* 2021;12(1):3770 doi: 10.1038/s41467-021-24109-5.

37. Conroy T, Desseigne F, Ychou M, Bouche O, Guimbaud R, Becouarn Y, et al. FOLFIRINOX versus gemcitabine for metastatic pancreatic cancer. *N Engl J Med* 2011;364(19):1817–25 doi 10.1056/NEJMoa1011923. [PubMed: 21561347]
38. Moore MJ, Goldstein D, Hamm J, Figer A, Hecht JR, Gallinger S, et al. Erlotinib plus gemcitabine compared with gemcitabine alone in patients with advanced pancreatic cancer: a phase III trial of the National Cancer Institute of Canada Clinical Trials Group. *J Clin Oncol* 2007;25(15):1960–6 doi 10.1200/JCO.2006.07.9525. [PubMed: 17452677]
39. Kindler HL, Niedzwiecki D, Hollis D, Sutherland S, Schrag D, Hurwitz H, et al. Gemcitabine plus bevacizumab compared with gemcitabine plus placebo in patients with advanced pancreatic cancer: phase III trial of the Cancer and Leukemia Group B (CALGB 80303). *J Clin Oncol* 2010;28(22):3617–22 doi 10.1200/JCO.2010.28.1386. [PubMed: 20606091]
40. Golan T, Hammel P, Reni M, Van Cutsem E, Macarulla T, Hall MJ, et al. Maintenance Olaparib for Germline BRCA-Mutated Metastatic Pancreatic Cancer. *N Engl J Med* 2019;381(4):317–27 doi 10.1056/NEJMoa1903387. [PubMed: 31157963]
41. Schram A, O'Reilly E, Somwar R, Benayed R, Shameem S, Chauhan T, et al. Clinical proof of concept for MCLA-128, a bispecific HER2/3 antibody therapy, in NRG1 fusion-positive cancers [abstract]. *Mol Cancer Ther* 2019;18(12 (Supl)):Abstract nr PR02 doi 10.1158/1535-7163.TARG-19-PR02.
42. Sequist LV, Yang JC, Yamamoto N, O'Byrne K, Hirsh V, Mok T, et al. Phase III study of afatinib or cisplatin plus pemetrexed in patients with metastatic lung adenocarcinoma with EGFR mutations. *J Clin Oncol* 2013;31(27):3327–34 doi 10.1200/JCO.2012.44.2806. [PubMed: 23816960]
43. Gan HK, Millward M, Jalving M, Garrido-Laguna I, Lickliter JD, Schellens JHM, et al. A Phase I, First-in-Human Study of GSK2849330, an Anti-HER3 Monoclonal Antibody, in HER3-Expressing Solid Tumors. *Oncologist* 2021;26(10):e1844–e53 doi 10.1002/onco.13860. [PubMed: 34132450]
44. Soule HD, Vazquez J, Long A, Albert S, Brennan M. A human cell line from a pleural effusion derived from a breast carcinoma. *J Natl Cancer Inst* 1973;51(5):1409–16 doi 10.1093/jnci/51.5.1409. [PubMed: 4357757]
45. Corsello SM, Bittker JA, Liu Z, Gould J, McCarren P, Hirschman JE, et al. The Drug Repurposing Hub: a next-generation drug library and information resource. *Nat Med* 2017;23(4):405–8 doi 10.1038/nm.4306. [PubMed: 28388612]
46. Sato M, Vaughan MB, Girard L, Peyton M, Lee W, Shames DS, et al. Multiple oncogenic changes (K-RAS(V12), p53 knockdown, mutant EGFRs, p16 bypass, telomerase) are not sufficient to confer a full malignant phenotype on human bronchial epithelial cells. *Cancer Res* 2006;66(4):2116–28. [PubMed: 16489012]
47. Li GG, Somwar R, Joseph J, Smith RS, Hayashi T, Martin L, et al. Antitumor Activity of RXDX-105 in Multiple Cancer Types with RET Rearrangements or Mutations. *Clin Cancer Res* 2017;23(12):2981–90 doi 10.1158/1078-0432.CCR-16-1887. [PubMed: 28011461]
48. Furukawa T, Duguid WP, Rosenberg L, Viallet J, Galloway DA, Tsao MS. Long-term culture and immortalization of epithelial cells from normal adult human pancreatic ducts transfected by the E6E7 gene of human papilloma virus 16. *Am J Pathol* 1996;148(6):1763–70. [PubMed: 8669463]

Statement of significance

NRG1 rearrangements encode chimeric ligands that activate the ERBB receptor tyrosine kinase family. Here we show that targeting HER2 and HER3 simultaneously with the bispecific antibody Zeno leads to durable clinical responses in patients with *NRG1* fusion-positive cancers, and is thus an effective therapeutic strategy.

Author Manuscript

Author Manuscript

Author Manuscript

Author Manuscript

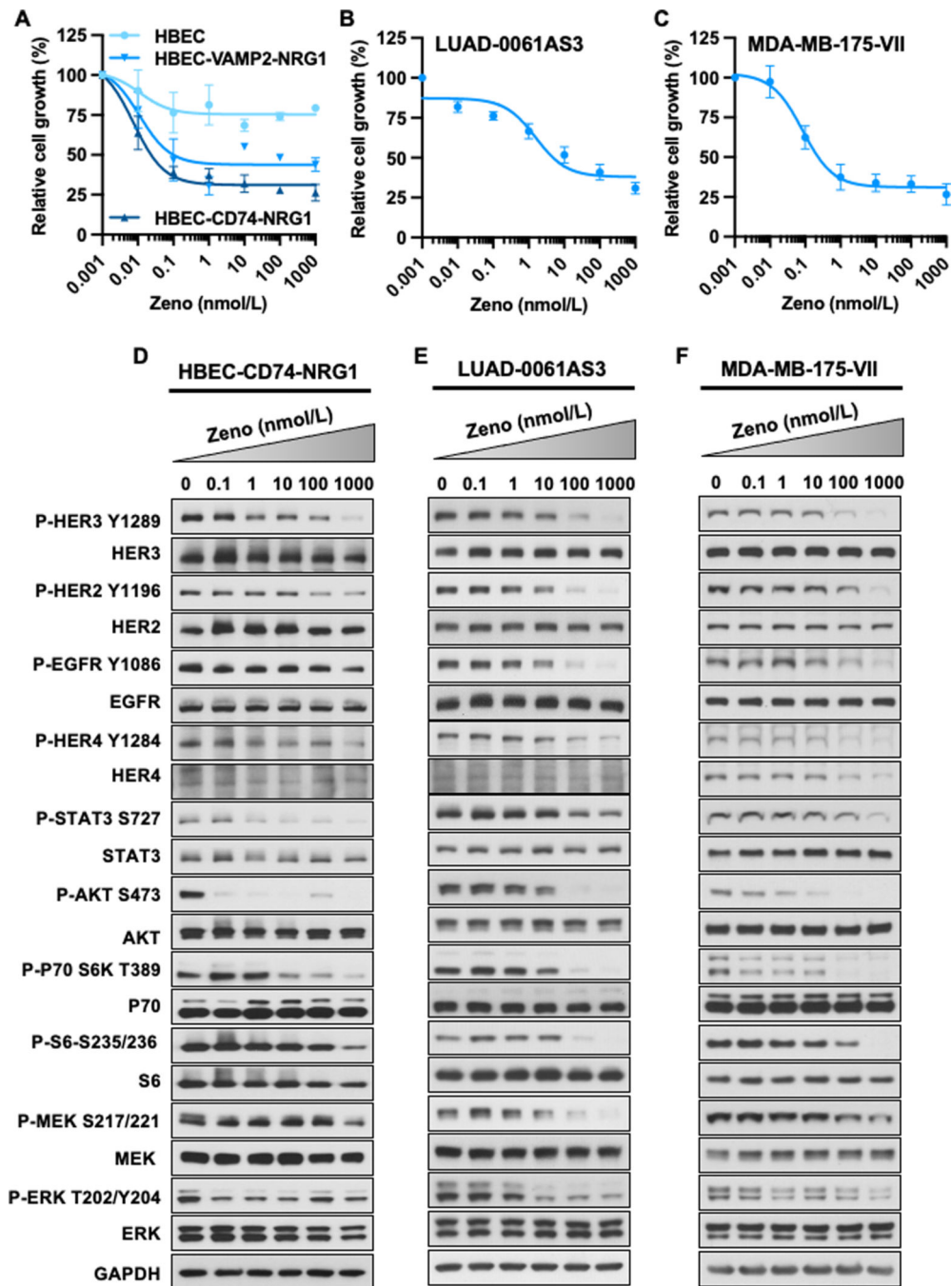


Figure 1. Zeno inhibits growth and blocks signal transduction in cell lines with *NRG1* fusions. **A-C.** Cells were treated with the indicated concentrations of Zeno for 96 h and then growth was determined using AlamarBlue viability dye. Values are expressed relative to the vehicle-treated control (100%). Data were analyzed by non-linear regression to determine IC_{50} for inhibition of growth (see Supplementary Fig. 2A for IC_{50} values). Results represent the mean \pm SD of three replicate determinations in one experiment. **D-F.** For Western blot analyses, cells were deprived of serum for 24 h and then treated with the indicated concentrations of Zeno for 1.5 hours prior to preparation of whole-cell extracts and

immunoblotting. Representative immunoblots are shown with GAPDH expression used as a western blotting loading control. At least two independent experiments were conducted.

Author Manuscript

Author Manuscript

Author Manuscript

Author Manuscript

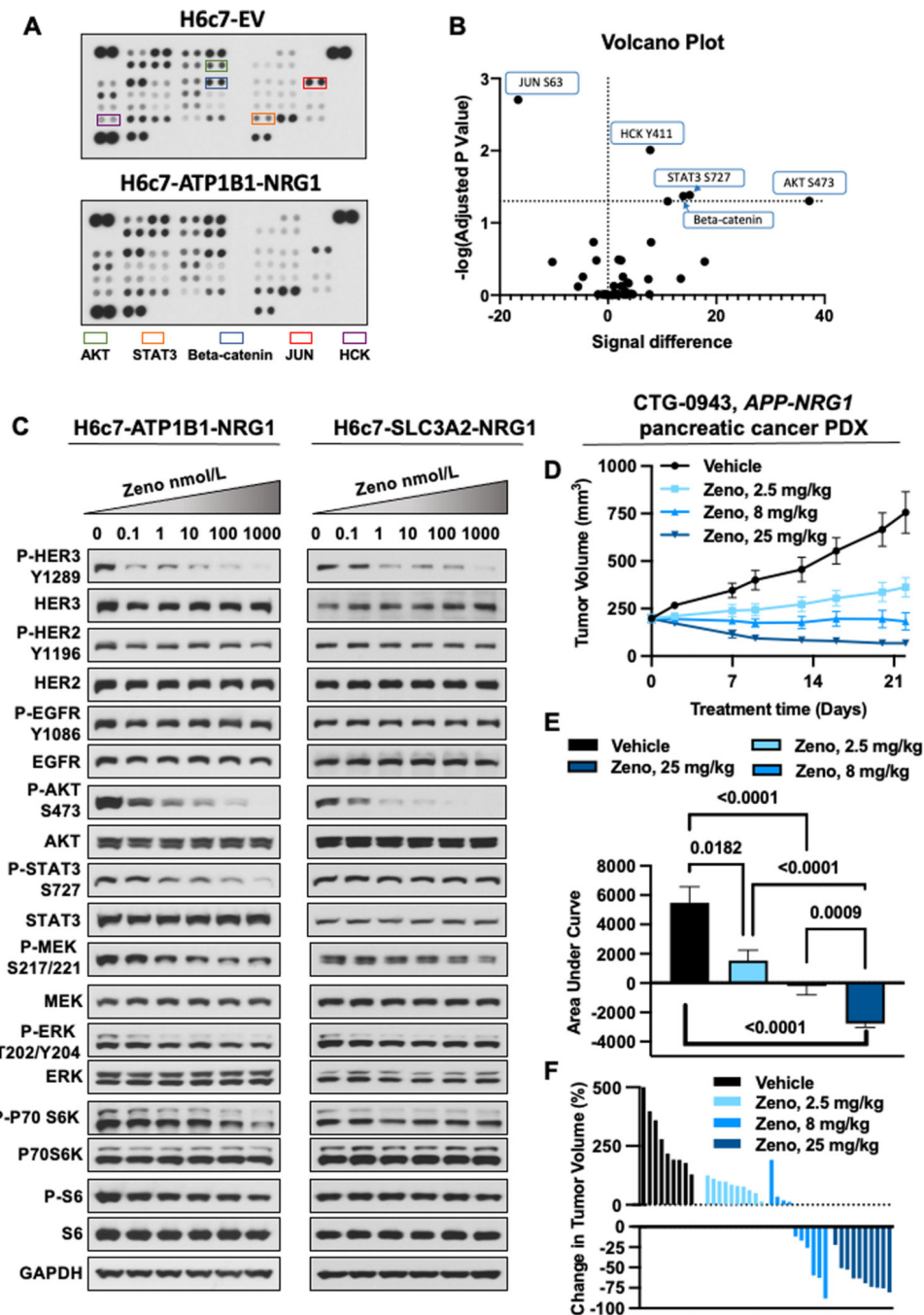


Figure 2. Zeno is effective in preclinical pancreatic cancer models.

NRG1 fusion cDNAs were expressed in the immortalized pancreatic ductal epithelial cell line H6c7. **A**. Phosphokinase array showing kinases activated in H6c7 cells expressing an empty vector (EV) or ATP1B1-NRG1 fusion. **B**. The arrays in A were quantitated by densitometry and a volcano plot of phosphorylation and p-value data is shown. Data above the horizontal dashed line represents a significantly different level of phosphorylation. Increased phosphorylation is shown to the right of the vertical dashed line, decreased phosphorylation to the left. **C**. H6c7-ATP1B1-NRG1 and H6c7-SLC3A2-NRG1 cells were

serum starved for 24 hours and then treated with Zeno for 1.5 h. Whole cell extracts were then prepared and subjected to western blotting. Representative immunoblots are shown with GAPDH expression used as a western blotting loading control. At least two independent experiments were conducted. **D-F**. A pancreatic adenocarcinoma PDX model (CTG-0943) was treated with the indicated dose of Zeno weekly. There were 10 animals per group. Tumor volume over time is shown in **D**. Area under curve analysis of tumor volumes is shown in **E**. **** $P < 0.0001$. There was no statistically significant difference between the Zeno-treated groups. The percent change in volume of individual tumors is shown in **F**.

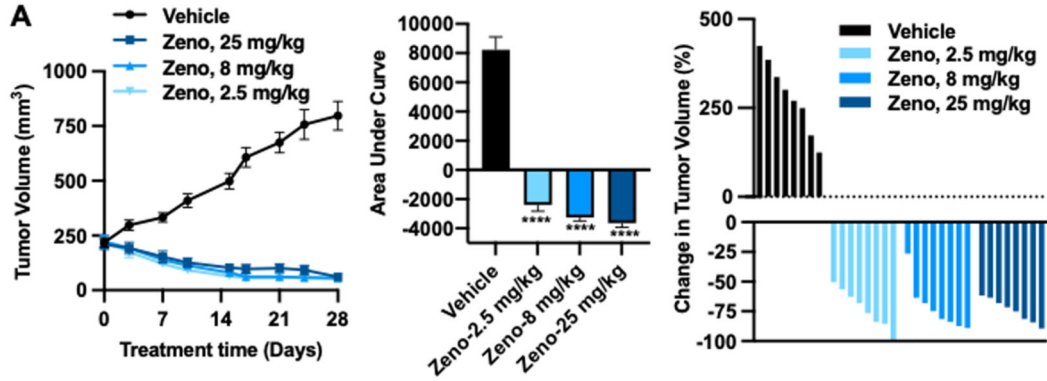
Author Manuscript

Author Manuscript

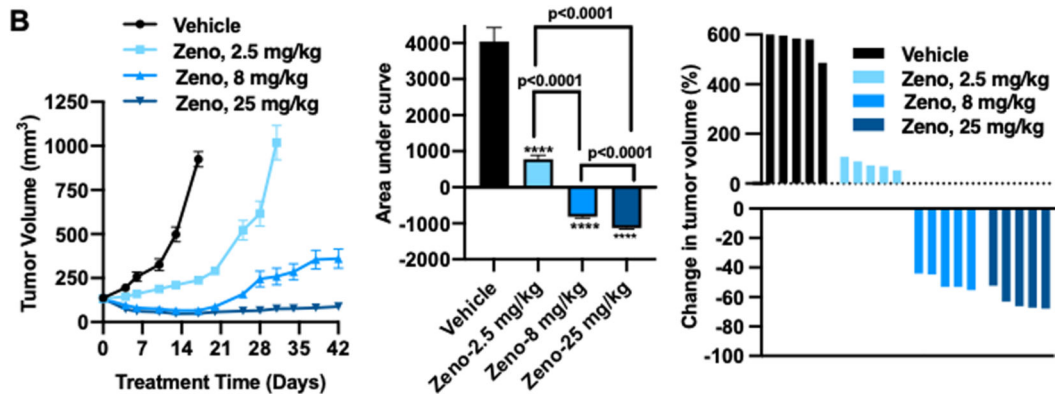
Author Manuscript

Author Manuscript

ST3204, *CD74-*NRG1**, lung cancer PDX



LUAD-0061AS3, *SLC3A2-*NRG1**, lung cancer PDX



OV-10-0050, *CLU-*NRG1**, ovarian cancer PDX

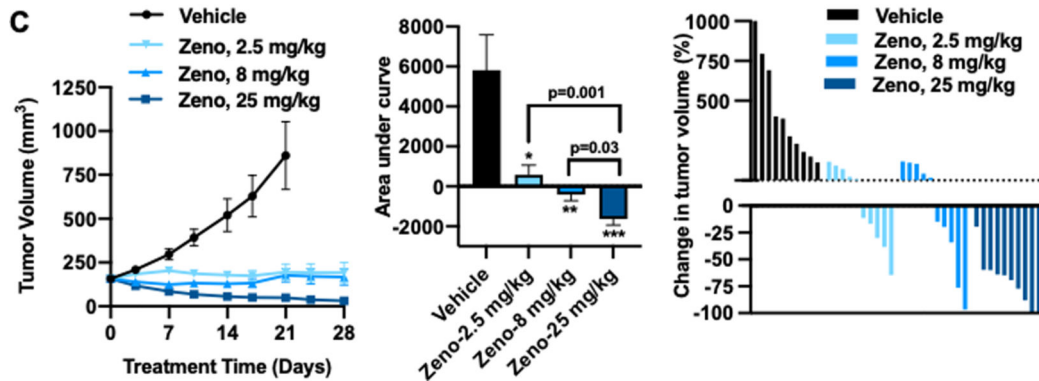


Figure 3. Zeno induces tumor regression in PDX models of *NRG1*-rearranged cancers. Mice bearing PDX tumors were treated with the indicated doses of Zeno once weekly. For each model, the figure shows the tumor volume (left panel), area under the curve analysis (AUC, middle panel), and the change in volume of individual tumors at the time representative of the AUC analysis (right panel). **A.** ST3204 PDX model (lung cancer; eight mice per group). AUC analysis was performed for the time period ending on day 28. Tumor growth in Zeno-treated animals was significantly lower than that in vehicle-treated animals as measured by AUC (**** P <0.0001), with no significant difference between the

AUC values of the Zeno-treated groups ($P>0.05$). **B.** LUAD-0061AS3 PDX model (lung cancer; five mice per group). AUC analysis was performed for the time period ending on day 17. **** $P<0.0001$ compared with the vehicle-treated group. **C.** OV-10-0050 PDX model (high-grade serous ovarian cancer; 10 mice per group). AUC analysis was performed for the time period ending on day 21. * $P=0.03$, ** $P=0.006$, *** $P=0.0006$ compared with the vehicle-treated group. Results in all left and middle panels represent mean \pm SEM. Administration of Zeno had no adverse effect on animal weight during the course of treatment (Supplementary Figure S4).

Author Manuscript

Author Manuscript

Author Manuscript

Author Manuscript

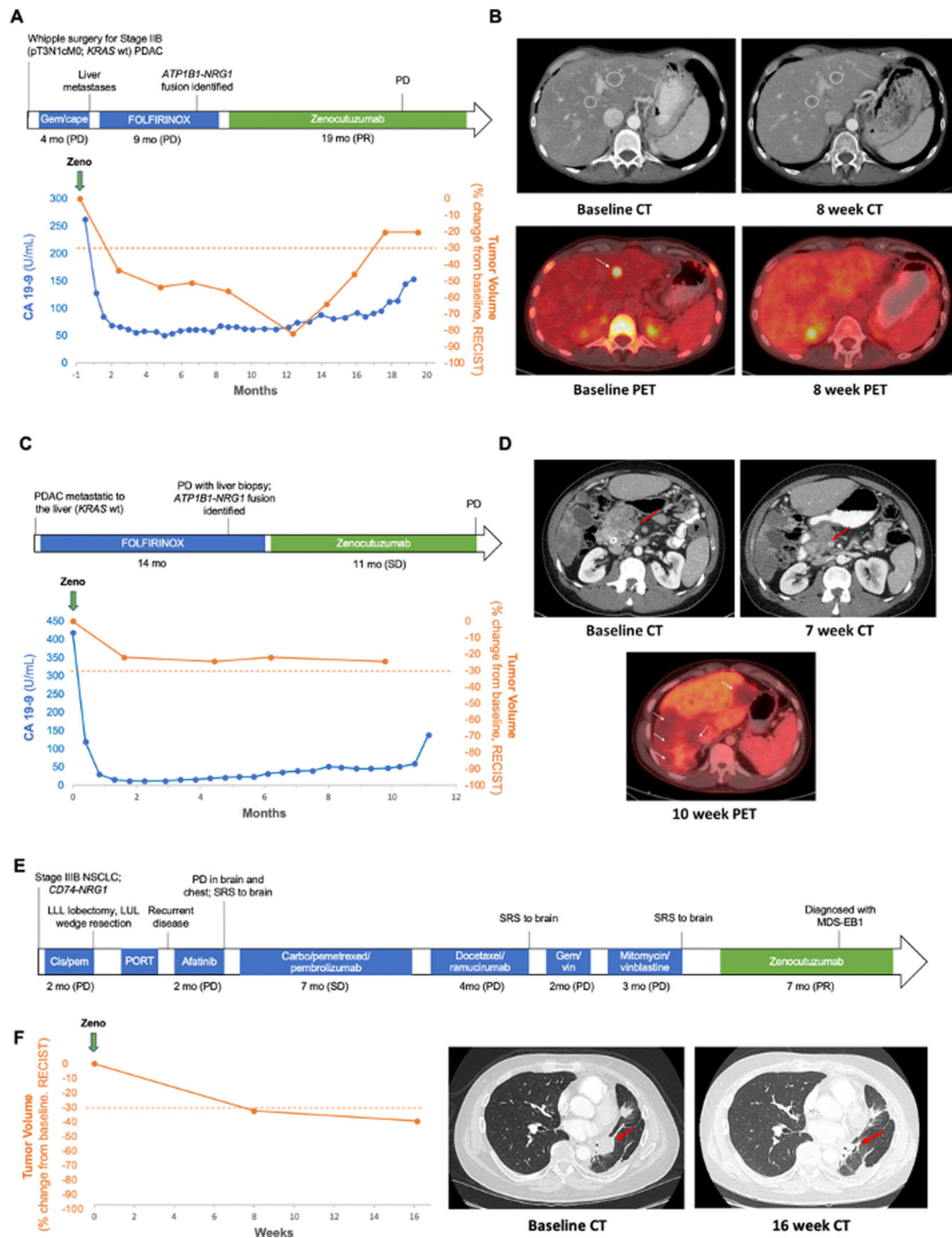


Figure 4. Clinical responses to Zeno.

A. Clinical course of a 50-year-old man with *ATP1B1-NRG1* fusion-positive PDAC treated with Zeno (top) including tumor volume and CA 19–9 levels during Zeno treatment (bottom). Best overall response is indicated for each therapy, including progressive clinical disease (PD) and partial response (PR) as defined by RECIST v1.1. **B.** Representative tumor imaging of this patient’s liver metastases at baseline and eight weeks into treatment with Zeno. **C.** Clinical course of a 34-year-old man with *ATP1B1-NRG1* fusion-positive PDAC treated with Zeno (top) including tumor volume and CA 19–9 levels during Zeno

treatment (bottom). Best overall response is indicated for Zeno [stable disease (SD) as defined by RECIST v1.1]. D. Representative tumor imaging from this patient showing a CT scan of the pancreas performed at baseline and seven weeks into treatment with Zeno, and a PET scan 10 weeks into treatment showing non-FDG avid liver metastases (no baseline available). E. Clinical course of a 52-year-old man with CD74-NRG1 fusion-positive NSCLC treated with Zeno after six prior lines of systemic therapy and multiple courses of radiation. Best overall response is labeled for each therapy, including clinical PD/SD, and PR as defined by RECIST v1.1. F. Tumor shrinkage in this patient depicted graphically (left) and by representative tumor imaging (right) performed at baseline and 16 weeks into Zeno treatment. Abbreviations: cape, capecitabine; carbo, carboplatin; gem, gemcitabine; MDS-EB1, myelodysplastic syndrome with excess blasts-1; pem, pemetrexed; PORT, post-operative radiation therapy; vin, vinorelbine.

Author Manuscript

Author Manuscript

Author Manuscript

Author Manuscript